

CrystEngComm

Accepted Manuscript



This is an *Accepted Manuscript*, which has been through the Royal Society of Chemistry peer review process and has been accepted for publication.

Accepted Manuscripts are published online shortly after acceptance, before technical editing, formatting and proof reading. Using this free service, authors can make their results available to the community, in citable form, before we publish the edited article. We will replace this *Accepted Manuscript* with the edited and formatted *Advance Article* as soon as it is available.

You can find more information about *Accepted Manuscripts* in the [Information for Authors](#).

Please note that technical editing may introduce minor changes to the text and/or graphics, which may alter content. The journal's standard [Terms & Conditions](#) and the [Ethical guidelines](#) still apply. In no event shall the Royal Society of Chemistry be held responsible for any errors or omissions in this *Accepted Manuscript* or any consequences arising from the use of any information it contains.

Cite this: DOI: 10.1039/c0xx00000x

www.rsc.org/crystengcomm

PAPER

Ultrasensitive and ultrasensitive TEA sensor based on α -MoO₃ hierarchical nanostructures and the sensing mechanism†

Lili Sui,^{ab} Xiaoxiao Song,^a Xiaoli Cheng,^a Xianfa Zhang,^a Yingming Xu,^{*a} Shan Gao,^a Ping Wang,^{ab} Hui Zhao^a and Lihua Huo^{*a}

5 Received (in XXX, XXX) Xth XXXXXXXXX 201X, Accepted Xth XXXXXXXXX 201X

DOI: 10.1039/b000000x

Flower-like, hierarchically nanostructured α -MoO₃ were successfully synthesized via a one-step, template-free solvothermal route. Morphological characterization demonstrated that the nanostructures were hierarchically assembled by overlapped single-crystalline nanobelts with exposed (010) facets.

10 These nanobelts with width of 40-60 nm and thickness of 20-30 nm grew radially from the core of α -MoO₃ flower. The growth mechanism of α -MoO₃ flower was speculated to be oriented self-attachments of nanobelts. The gas sensor based on α -MoO₃ flowers showed an excellent sensing performance to triethylamine (TEA) in terms of high response (931.2) and excellent selectivity to 10 ppm TEA. Especially, the detection limit was down to 0.001 ppm at a working temperature of 170°C. The surface
15 status of α -MoO₃ flowers before and after exposure to TEA at 170°C were investigated by XPS. Probable oxidation product of TEA was analyzed by GC-MS. The MoO₃ sensing mechanism could be interpreted as the transformation of triethylamine to vinylamine through two catalytic oxidation processes: reaction with chemisorbed oxygen and lattice oxygen. The possibility related to enhanced gas sensing response of the three-dimensional (3D) flower-like α -MoO₃ was discussed.

20 Introduction

Increasing harmful, toxic and combustible gases released from factories and living environment have been global environmental issues. It is urgent to accomplish fast, effective and real-time monitoring hazardous gases by virtue of high-performance gas
25 sensors. Nanostructured materials, especially metal oxide semiconductors (MOS) with controlled structure and dimension, have been widely applied in chemical gas sensors to enhance gas sensing properties because of their high sensitivity.¹ Many semiconducting metal oxides such as SnO₂, WO₃, Fe₂O₃, ZnO
30 and In₂O₃, have been extensively investigated, they showed excellent sensitivity and response speed.²⁻⁶ But the defect of poor selectivity limits their practical application under complex surrounding conditions.

As one of the most significant functional materials, MoO₃ is an
35 environmentally friendly n-type semiconductor material ($E_g = 3.1$ eV), which has attracted considerable attention in the field of photocatalysts,^{7,8} gas sensors,^{9,10} electrochemistry,^{11,12} field emission,¹³ gaschromic¹⁴ and photochromic devices¹⁵ due to its special quantum size effect, surface effect and high reactivity
40 characteristics. Among three basic polymorphs of MoO₃, orthorhombic MoO₃ (α -MoO₃) has good thermal stability, and the unique layered crystal structure is favorable for gases to diffuse, thus, α -MoO₃ is a kind of promising candidate for gas sensor.

To date, the reported gas sensing studies of MoO₃ still mainly
45 focused on low-dimensional nanostructures, such as zero-

dimensional (0D) nanoparticles, one-dimensional (1D) nanowires and nanorods, and two-dimensional (2D) nanoplates, which have been used to fabricate gas sensors for detection of H₂, NH₃, C₂H₅OH, NO, NO₂, CO, CH₄ and (CH₃)₃N (TMA).¹⁶⁻²²
50 Triethylamine (TEA) is a kind of volatile organic compound (VOC) and widely used as organic solvent and catalyst in the industrial production, but it easily generates risks to environment due to its toxic, inflammable and explosive nature, and exhibits a great damage on respiratory, causing pulmonary edema and even
55 death.²³ It is also released gas during the decay of fishes and seashells after death.²⁴⁻²⁶ It is recommended that the permissible exposure limit of TEA in the workplace is 10 ppm by National Institute for Occupational Safety and Health (NIOSH), and the threshold limit value (TLV) is 1 ppm established by American
60 Conference of Governmental Industrial Hygienists (ACGIH).²⁶ So it is necessary to use highly sensitive chemical sensors for accomplishing rapid and real-time detection of sub-ppm, even sub-ppb level TEA in the industrial processes, fish processing industries and complex surrounding conditions.

65 It has indicated that gas sensing behavior depends on the adsorption of tested gases on the sensing layer and their subsequent reaction with the sensing materials, that means, surface morphology and architecture of sensing materials have significant effect on the gas sensing properties. Among various
70 morphological structures, three-dimensional (3D) hierarchical nanostructures assembled from low dimensional nano-building blocks have attracted much attention owing to their large specific surface areas and low agglomerated configurations, which allow

effective gas diffusion and charge transport. It has shown that various hierarchical metal oxides such as SnO₂, ZnO, WO₃, Fe₂O₃, In₂O₃, NiO, Co₃O₄ etc., can accomplish the improvement of the sensitivity, selectivity or response speed.²⁷⁻³⁵ As well, much effort has been given to prepare various 3D hierarchical MoO₃ structures assembled by 1D nanobelts, nanorods and nanorods arrays, 2D nanosheets, via wet chemistry method, hydrothermal route, microwave hydrothermal method and electrodeposition strategy.³⁶⁻⁴¹ Most of the above processes are usually complicated or need surfactants and templates, which have to undergo complex removal procedures. Moreover, the present works so far mainly focus on the fundamental research of synthesis methods and formation process, while the properties, especially the gas sensing performance and related sensing mechanism of the hierarchical α -MoO₃ nanostructures have rarely been reported. A solvothermal route combined with subsequent calcination in air was realized as an effective approach to prepare hierarchical MoO₃ flowers just recently,⁴² the building-blocks of which were polycrystalline microrods. The sensor based on such α -MoO₃ flowers exhibited excellent gas sensing performance to TEA gas, but the relatively higher working temperature (250 °C) and detection limit (0.5 ppm) still need to be improved. A few investigations show that some metal oxide semiconductors with exposed high-index facets could effectively improve the physiochemical properties in the applications of lithium ion batteries,^{43,44} photocatalysts⁴⁵ and gas sensors,^{46,47} because the exposed special facets possessed higher surface energies, more atom terraces and dangling bonds than those with low-index facets. In order to further improve the TEA sensing performance of α -MoO₃, it is strongly desirable for fabrication well-defined hierarchical α -MoO₃ nanomaterials, especially constructed by oriented building units with exposed high-index facets, via simpler route and corresponding investigation of the gas sensing performance and mechanism.

Herein, hierarchical flower-like α -MoO₃ was prepared via a one-step solvothermal method, the 3D hierarchical nanostructure constructed by 1D single-crystalline nanobelts with exposed (010) facets achieved ultrasensitive, ultrasensitive and reliable detection of TEA at 170 °C. The gas sensing performance of three different morphologies of α -MoO₃ and their relationships were investigated. Moreover, the TEA sensing mechanism of α -MoO₃ flowers was further explored, and a new mechanism model was suggested.

Experimental

Synthesis of α -MoO₃ materials

All chemicals were of analytical grade and used without further purification. Hierarchical α -MoO₃ flowers were prepared by a solvothermal synthesis route. Typically, 0.114 g of molybdenyl acetylacetonate (C₁₀H₁₄MoO₆) was ultrasonically dispersed in a mixture of acetic acid (33 mL) and distilled water (2 mL), and then stirred for 30 min to form a uniform emulsion. The resulting emulsion was transferred into 50 mL Teflon-lined stainless steel autoclave, which was then sealed and heated at 150 °C for 8 h. After cooling down to room temperature, the obtained precipitates were centrifuged, rinsed several times with deionized water and ethanol, respectively, and dried at 60 °C for 12 h.

Moreover, to investigate the formation of the hierarchical α -MoO₃ flowers, a series of control experiments were carried out by changing the reaction time during the solvothermal reaction process. For comparison the gas sensing properties, α -MoO₃ nanoparticles and nanobelts were also prepared at the reaction time of 5 min and 30 min, respectively, other synthesis conditions were the same as those of α -MoO₃ flowers.

Characterization

The phase and crystal structure of the as-synthesized samples were characterized by X-ray powder diffraction meter (XRD, D/MAX-III-B-40KV, Japan, Cu-K α radiation, $\lambda=1.5406$ Å). The morphology and microstructure of the products were observed by scanning electron microscope (SEM, HITACHI S-4800) with an acceleration voltage of 5 kV and transmission electron microscope (TEM, JEOL, JEM-2100) with an acceleration voltage of 200 kV. Fourier transform infrared spectra (FT-IR) of the samples were recorded with KBr pellets using a FT-IR spectrometer (Bruker Equinox, 55) with a mercury-cadmium-telluride (MCT) detector. Thermogravimetric (TG) analysis was performed on a thermogravimetric analyzer (Perkin Elmer, TG/DTA 6300) from 25 to 900 °C at a heating rate of 20 °C min⁻¹ in air flow. The standard TEA and intermediate gaseous product after the α -MoO₃ flowers sensor exposed to TEA was monitored by gas chromatography-mass spectrometer (GC-MS, AGILENT, 6890-5973N) using a DB-5 (30 m \times 0.25 mm \times 0.25 μ m, AGILENT) column from 50 to 250 °C at a heating rate of 10 °C min⁻¹ in N₂ flow rate of 1 mL min⁻¹. The sample was also analyzed by X-ray photoelectron spectroscopy (XPS) (VG Scientific, ESCALAB 250) with Al K α radiation ($h\nu = 1486.6$ eV) within ± 0.2 eV deviation in the binding energy position.

Fabrication of gas sensors

The as-obtained α -MoO₃ nanoparticles (Mo-NP), nanobelts (Mo-NB) and flowers (Mo-FL) were uniformly dispersed into a small amount of terpineol, respectively, to form α -MoO₃ pastes, which were then painted on the surface of Al₂O₃ microtubes (4 mm in length, 1.2 mm in external diameter and 0.8 mm in internal diameter) with a pair of Au electrodes attached with Pt wires. A heater of Ni-Cr wire was inserted into the Al₂O₃ microtube to control the working temperature and housed on a six probe circular contact. These sensors were connected to the pins by welding, and the completed sensors housed with the ceramic sensor was inserted into the six pins socket and connected to a sensor-test system.⁴⁸ Before sensing measurement, as-prepared sensors were aged on aging equipment at 350 °C for 3 days to improve the stability of the sensors.

Measurement of gas sensing performance

Measurements on gas response were performed with a JF02E sensor test system (Kunming, China) at different temperatures by a DC method. The gas sensing measurement of the sensor was carried out in a static system by the method reported previously.⁴⁸ Before measurement, a 10 L glass chamber was evacuated by pump in advance, and then the tested organic liquid (or gas) was injected into the container by a syringe. After the liquid was volatilized totally by heating, air with 25 \pm 5 RH% was used as the dilute gas and passed into the container to balance the pressure of the inner and outer of container. The gas response can

be measured when the sensor was put in/taken out of the gas container. Detailed operating process can be found in Ref. 49. During the measurement, the temperature and the relative humidity of the test chamber were 24 ± 1 °C and 25 ± 5 RH%, respectively. The sensor response (S) is defined as $S = R_a/R_g$, where R_a and R_g are the sensor resistances in air and in test gas, respectively. The response/recovery time is defined as the time needed to reach 90% of total signal change.

Results and discussion

10 Morphology and composition

The morphology and refinement structure of the as-prepared sample after solvothermal reaction for 8 h were examined by SEM and TEM techniques. Fig. 1a is the SEM image of the product, showing the diameters of the flowers about 10 μm . And from the high-magnification SEM image (Fig. 1b and c), it is clearly observed that numerous nanobelts with sharp tips and rough rims linked to one center are 20-30 nm in thickness. These high-density nanobelts are radially assembled into flower-like shape, which is named as the flower-like hierarchical nanostructures. The fine nanostructures of the as-obtained sample were performed by TEM (Fig. 2). As the low-magnification TEM images (Fig. 2a and b) show, the constructed hierarchical nanostructures consist of dense nanobelts with similar width (40-60 nm) and length (2-3 μm), growing radially from the core of the flower and overlapping closely with each other. The result is consistent well with the SEM observation. Furthermore, the HRTEM image (Fig. 2c) demonstrates that the lattice fringes with interplanar spacing of approximate 0.39 nm correspond to the (100) plane of the orthorhombic phase of $\alpha\text{-MoO}_3$. From the perspective of energy, the rates of planar growth along the axes of $\alpha\text{-MoO}_3$ crystal are in the following order: [001], [100], [010],^{12,43} implying the preferential growth of the nanobelts are along [001] direction. Meanwhile, the selected area electron diffraction (SAED) pattern (inset of Fig. 2c) recorded perpendicular to the growth axis of the belts can be indexed to the [010] zone of $\alpha\text{-MoO}_3$, which indicates the single crystal nature and further confirms the favored [001] growth direction. In detail, the (010) planes and the (100) planes encircle the nanobelt facets along the longitudinal direction, and the (001) planes enclose both ends. Thus the largest exposed surfaces are (010) facets, as shown in Fig. 2d.

The structure and phase purity of the sample was also investigated by XRD. The XRD pattern (Fig. 3a) of the flowers shows that all the diffraction peaks can be indexed to the orthorhombic phase of MoO_3 (JCPDS card No. 05-0508, space group: Pbnm (62), $a = 3.962$ Å, $b = 13.858$ Å, $c = 3.697$ Å). The absence of notable impurity phases and the sharp diffraction peaks suggest that $\alpha\text{-MoO}_3$ product with high crystalline purity is obtained.

FT-IR spectrum of the product is shown in Fig. 3b. There are five main peaks at 553, 836, 1003, 1621 and 3441 cm^{-1} , respectively. The peaks in the region from 500 to 1000 cm^{-1} are attributed to Mo–O stretching vibration modes. The peak observed at 553 cm^{-1} is ascribed to the triply coordinated oxygen ($\text{Mo}_3\text{-O}$) stretching mode, while the peak at 836 cm^{-1} is assigned to the doubly coordinated oxygen ($\text{Mo}_2\text{-O}$) stretching vibrations.

The band located at 1003 cm^{-1} is due to the stretching vibration of Mo=O, which is an indicator of the layered orthorhombic $\alpha\text{-MoO}_3$ phase.^{9,50} Moreover, the peaks at 3441 and 1621 cm^{-1} correspond to the O–H stretching and bending vibration of the trace water molecules adsorbed on MoO_3 , respectively.⁵⁰ Hence, the FT-IR result together with the XRD result confirms that the as-obtained product is pure phase of $\alpha\text{-MoO}_3$.

Growth mechanism

To investigate the growing process of $\alpha\text{-MoO}_3$ flower, time-dependent experiments were carried out and investigated by TEM technique (see Fig. 4). Fig. 4a shows a typical TEM image of the sample synthesized at 150 °C for 5 min. It can be seen that many nanoparticles with the diameter of 40 nm formed. When the time of solvothermal reaction was up to 30 min, the product was composed of nanobelts of about 50 nm in width, closely overlapping with each other, as shown in Fig. 4b. Upon increasing the reaction time to 2 h, most of the belts gathered together and further star-like nanostructures formed (Fig. 4c). When the reaction time was prolonged to 8 h, $\alpha\text{-MoO}_3$ flowers appeared, which were constructed with the building units of close-packed nanobelts, as shown in Fig. 4d. To sum up, the formation of the 3D flower-like $\alpha\text{-MoO}_3$ hierarchical nanostructures might experience the following evaluation process: 0D nanoparticles \rightarrow 1D nanobelts \rightarrow 3D flowers.

The corresponding XRD patterns of the 0D nanoparticles and 1D nanobelts are shown in Fig. S1 as curve (a) and curve (b), respectively, all of the diffraction peaks can be perfectly assigned to orthorhombic $\alpha\text{-MoO}_3$ (JCPDS card No. 05-0508). The nanobelts formed at the reaction time of 30 min are the building-blocks of the $\alpha\text{-MoO}_3$ flowers, the three marked diffraction peaks of (020), (040) and (060) in curve (b) suggest a highly anisotropic growth in the $[0k0]$ direction, which reveals the favorable crystal direction.^{12,38,43} This confirms the result that obtained from the HRTEM analysis. However, it should be mentioned that the relative intensities of diffraction peaks of the $\alpha\text{-MoO}_3$ flowers (Fig. 3a) are different from those of the nanobelts (Fig. S1 curve (b)), particularly the prominent (021) diffraction peak of the $\alpha\text{-MoO}_3$ flowers might be attributed to the 3D hierarchical micro/nanostructures.

On the basis of above information, the growth mechanism of flower-like $\alpha\text{-MoO}_3$ hierarchical nanostructures could be illustrated by the scheme in Fig. 4. In the first step, the initial nanoparticles formed under the proper acidic condition by conventional nucleation. Subsequently, these nanoparticles dissolved and recrystallized into nanobelts along the [001] preferential orientation as the reaction solution reached its solubility limit, which was favorable to reduce the interfacial energy from the viewpoint of energy, thus the nanobelts with largest exposed surfaces of (010) facets formed. Then, these nanobelts regularly stacked with each other as the reaction went on, and the oriented attachment of these nanobelts resulted in the formation of loose star-like nanostructures. At the final stage, the developed flower-like $\alpha\text{-MoO}_3$ hierarchical nanostructures gradually formed through further oriented attachment and self-assembly process.

Gas sensing properties

In order to investigate the effect of morphology on the sensing properties of α -MoO₃ nanostructures, three sensors based on nanoparticles (Mo-NP), nanobelts (Mo-NB) and flowers (Mo-FL) were fabricated, whose sensing materials were obtained after solvothermal reaction at 150 °C for 5 min, 30 min and 8 h, respectively. Fig. 5a shows the temperature-dependent response measurements of the three sensors towards 10 ppm TEA. Obviously, the responses of these three morphologies of α -MoO₃ to 10 ppm TEA at 170-290 °C present the same variation trend with the working temperature increasing, that is, the responses of these sensors to TEA decrease with working temperature increasing from 170 to 290 °C, which might be attributed to the characteristics of the sensing materials and adsorption/desorption quantities of TEA molecules on the surface of α -MoO₃. When the α -MoO₃ sensor is exposed to 10 ppm TEA gas at 170 °C, more TEA gas molecules are adsorbed on the α -MoO₃ surface and oxidized, indicating high activity of the reaction at the relatively low working temperature of 170 °C. However, with the temperature increasing, more and more TEA molecules are much easier to be desorbed from MoO₃ surface, leading to the effective adsorption quantities of TEA decrease. This results in the responses of the sensors gradually decreasing when the temperatures are higher than 170 °C. Because the resistances of these three sensors all exceed to the detection range of the test system when operated below 170 °C, 170 °C is chosen as the optimum working temperature of the three sensors, which is lowered 80 °C than that of our reported α -MoO₃ flowers.⁴²

Fig. 5b depicts the correlation between TEA concentrations and responses of the Mo-NP, Mo-NB and Mo-FL sensors operated at 170 °C. The responses of three sensors all increase with the gas concentration increasing in the entire concentration range of 0.001-10 ppm TEA, in which the responses of Mo-FL are all significantly higher than those of Mo-NP and Mo-NB with an increase of greater magnitude, especially in the higher concentration range. The response of Mo-FL sensor to 10 ppm TEA vapor is up to 931.2, about 8.1 and 33.7 times higher than those of Mo-NB (114.9) and Mo-NP (27.6), respectively. This value is also significantly superior to the response of those reported materials including CoFe₂O₄, SnO₂, NiFe₂O₄, α -Fe₂O₃, TiO₂, ZnO, V₂O₅ and our previous reported α -MoO₃ to the same concentration of TEA (Table 1).^{5,25,26,42,51-55} Also, the excellent sensing performance of Mo-FL is further demonstrated as the detection limit of 0.001 ppm at 170 °C, the response of which is 5.1, corresponding to the lowest detection limit of ZnO nanorods reported up to now.⁵ The TEA detection limit of Mo-NP and Mo-NB is 0.1 and 0.01 ppm, respectively, while that of our reported α -MoO₃ flowers is 0.5 ppm at 250 °C. In addition, there are good linear relationship (R^2) between the response of Mo-FL and TEA, $R^2 = 0.9993$ for 0.001-1 ppm and 0.9911 for 1-10 ppm TEA. Accordingly, the sensor based on as-obtained α -MoO₃ flowers can real-time monitor ppm level, even in ppb levels of TEA with a better wider and linear detection concentration range.

To quantify the selectivity of the α -MoO₃ sensors, the responses of the sensors to 10 ppm of ammonia (NH₃), chlorobenzene (C₆H₅Cl), acetone (C₃H₆O), ethanol (C₂H₅OH), dimethylamine ((CH₃)₂NH, DMA), trimethylamine ((CH₃)₃N, TMA) and triethylamine ((C₂H₅)₃N, TEA) gases were investigated at 170 °C and summarized in Fig. 5c. The Mo-NP, Mo-NB and Mo-FL

sensors show negligible sensitivity to 10 ppm of ammonia, chlorobenzene, acetone and ethanol, the responses are all less than 3.4. When exposed to 10 ppm TMA and DMA gases, the Mo-NP shows very weak responses of 3.3 and 2.2, the responses are about 8.6 and 12.3 for Mo-NB, and 21 and 32.7 for Mo-FL, respectively. However, the Mo-NP, Mo-NB and Mo-FL sensors all exhibit much higher response and selectivity to TEA compared with other gases. The high selectivity of the α -MoO₃ sensors to TEA might be ascribed to the characteristics of target gases and the effect of acid property of MoO₃ sensing material. Among the test gases of ammonia, chlorobenzene, acetone, ethanol, DMA, TMA and TEA, TEA has three ethyl groups, especially compared with the three hydrogen atoms in NH₃, and the two/three methyl groups in DMA/TMA, which provide it the largest electron-donating ability. Meanwhile, the nitrogen atom in TEA has a lone pair electrons that can donate to form bonds, thus, TEA is prefer to be adsorbed onto Lewis-acid (Mo ion) sites,¹⁹ especially at the optimum working temperature of 170 °C. The dynamic responses of the typical sensor based on Mo-FL during cyclic exposure to 0.001-10 ppm TEA at 170 °C are shown in Fig. 5d. The resistances decline instantly and reach to a minimum value when exposed to TEA, corresponding to the gas-sensing characteristics of n-type semiconductor oxides. Apparently, the transients exhibit rapid response characteristic and good reversibility. The corresponding response times of Mo-FL sensors to 0.001 ppm TEA is 31 s, and to 10 ppm TEA is 25 s which is a little shorter than those of Mo-NP (28 s) and Mo-NB (29 s) sensors. Fig. S2 a and b show the responses of the Mo-NP to 0.1-10 ppm and Mo-NB to 0.01-10 ppm TEA at 170 °C, respectively.

Compared with 0D Mo-NP and 1D Mo-NB sensors, especially our reported α -MoO₃ flowers,⁴² this 3D Mo-FL sensor exhibits either the highest sensitivity to TEA at different temperatures, different concentrations, or the highest selectivity and faster response to TEA at 170 °C. The enhanced sensing performance might be partly interpreted by the high-index (010) facets of the α -MoO₃ flowers because the special exposed facets can effectively improve the surface adsorption ability of the materials due to the improved surface reactivity.⁴⁷ Moreover, the specific surface area and the pore size distribution of the three α -MoO₃ samples were characterized by nitrogen sorptometer measurements, as shown in Fig. 6. The BET specific surface areas of Mo-NP, Mo-NB and Mo-FL are 11.5, 19.8 and 34.8 m² g⁻¹, respectively, thus, the 3D hierarchical flower-like α -MoO₃ can provide larger surface to volume ratio but less agglomeration of low dimensional nano-building blocks. In addition, the Mo-FL presents higher pore volumes than those of Mo-NP and Mo-NB over the entire pore diameter range (1-180 nm), which results in the higher gas-accessibility for more favorable gas molecules diffusion and adsorption on the surface of the 3D hierarchical flowers.

From the viewpoint of practical application, the stability of Mo-FL sensor was investigated to 10 ppm TEA at a working temperature of 170 °C under the same ambient condition of 25 ± 5 RH% (Fig. S3). Within 5 months, the Mo-FL sensor remains 97 ± 2% of their original response, confirming good long-term stability of the Mo-FL sensor. Such α -MoO₃ hierarchical flowers are good sensing candidates for ultrasensitive and fast monitoring trace TEA at 170 °C.

Gas sensing mechanism

The gas sensing mechanism can be speculated by virtue of the XPS and GC-MS techniques in this study.

The chemical state change of the Mo-FL sensor surface was analyzed by XPS before and after the sensor exposure to TEA as shown in Fig. 7. Before the sensor was exposed to TEA, the Mo 3d spectrum (Fig. 7a) shows two peaks at 232.4 and 235.6 eV, which are consistent with those of Mo⁶⁺ in MoO₃,⁵⁶ and the O 1s XPS spectrum (Fig. 7d) can be deconvoluted to three peaks corresponding to lattice oxygen (529.8 eV), surface adsorbed oxygen (531.4 eV) and hydroxyl oxygen (532.9 eV).⁵⁷ This result confirms the existence of chemisorbed oxygen, which is opposite to the recent report that MoO₃ did not chemisorb oxygen due to its peculiar layered structure.^{10,58} After the sensor is exposed to 0.01 ppm TEA at 170 °C, two peaks located at 232.7 and 235.9 eV are observed in Mo 3d spectrum (Fig. 7b),⁵⁶ indicating that the Mo⁶⁺ valence state is hardly changed. However, the percentage of surface adsorbed oxygen (Fig. 7e) decreases to 23% compared to the original 35% before the sensor is exposed to TEA (Fig. 7d). The result may demonstrate that the oxidation reaction only occurs between the adsorbed oxygen and detected reducing gas when the TEA concentration is below 0.01 ppm. Moreover, when the concentration of TEA increases to 10 ppm, Mo⁵⁺ can also be detected, which is confirmed by the appearance of the peaks Mo 3d5/2 (231.4 eV) and 3d3/2 (234.5 eV) as shown in Fig. 7c.⁵⁶ It suggests that partial reduction of Mo⁶⁺ to Mo⁵⁺ happens after the sensor exposure to 10 ppm TEA. Meanwhile, the percentage of chemisorbed oxygen on the sensor surface only accounts for 11% (Fig. 7f). Therefore, it is possible to conclude that main sensitive reaction between MoO₃ and TEA is TEA catalytically oxidized by the lattice oxygen of MoO₃ at high concentration gas, accompanying with the partial reduction of metal ion. And the higher concentration of TEA is, the more quantity of Mo⁶⁺ would be reduced to Mo⁵⁺.

In order to well understand the sensing mechanism of MoO₃ to TEA, it is necessary to ascertain the oxidation product after TEA contact to MoO₃. Thus far, there have been no effective ways for determining the oxidized or reduced product of target gases in gas sensing detection because of their gaseous state and trace amount. Here, we analyzed the gas composition and seized direct evidence of the intermediate gaseous product by GC-MS technique after the α -MoO₃ flowers sensor was exposed to TEA. Fig. S4 a shows representative standard chromatogram of TEA, the retention time (Rt) is 1.58 min, corresponding to the fragment m/z =101 in Fig. S4 b. When TEA contacts with α -MoO₃ flowers at 170 °C, new specimen produces whose Rt is 1.81 min (Fig. S4 c), relating to the intense ion with m/z =100 in the mass spectroscopy of Fig. S4 d. Thus, TEA may undergo a process of dehydrogenation, the m/z =100 could be speculated to be vinylamine (Et₂NH⁺—CH=CH₃), which was also found by De la Fuente⁵⁹ and Xu et al²³ under photocatalization process.

As mentioned above, in consideration of our investigation results and reported opinions, the gas sensing behaviors of α -MoO₃ towards TEA are directed by two courses: the surface reaction process (reaction with chemisorbed oxygen) is dominant at relatively low concentration of TEA and subsequently slow bulk (reaction with lattice oxygen) reaction process is advantageous with the concentration of TEA increasing. A

possible sensing mechanism of α -MoO₃ flowers towards TEA is represented as Fig. 8 and suggested as follows:

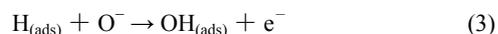
MoO₃ is an n-type semiconductor. When the sensor based on α -MoO₃ flowers is in air at 170 °C, oxygen molecules, adsorbed on the sensor surface, act as acceptor and capture electrons from the conduction band to form chemisorbed oxygen on grain boundaries in the form of O⁻ at the temperature range of 100–300 °C.⁶⁰ As a consequence, electron depletion layers form on the surface of α -MoO₃ nanobelts, shown as the process (a) in Fig. 8.



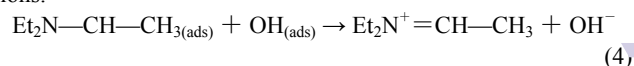
After the sensor is exposed to TEA gas, TEA molecules are adsorbed on the surface of the α -MoO₃ sensor, the C—H of methylene in TEA dissociates to yield the dehydrogenated neutral radical of amine and hydrogen with the catalysis of MoO₃, as shown below:



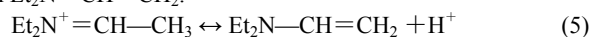
Subsequently, the chemisorbed oxygen O⁻ on α -MoO₃ surface is suggested to act as an electron donor, binds with the H atom to form the adsorbed hydroxyl group and releases electron in the mean time.



Then, electron transfer happens from Et₂N—CH—CH₃(ads) (Eq 2) to OH_(ads) (Eq 3), and generates the Et₂N⁺=CH—CH₃ and OH⁻ ions.



After that, the product Et₂N⁺=CH—CH₃ (Eq 4) loses H⁺ to form Et₂N—CH=CH₂.

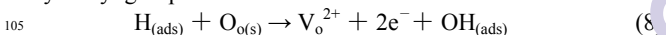


Finally, the produced OH⁻ (Eq 4) and H⁺ (Eq 5) combine into water.



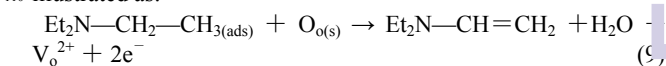
The sensitive process on the sensor surface is represented as the process (b) in Fig. 8. The overall reaction is presented as: Et₂N—CH₂—CH₃(ads) + O⁻(ads) → Et₂N—CH=CH₂ + H₂O + e⁻ (7)

Molybdenum oxides are known to be very good catalysts in oxidation reactions and may enhance the capability of adsorption and breakdown of TEA molecules at low working temperature of 170 °C in our gas sensing detection. Thus, when the concentration of TEA increases, more TEA molecules are adsorbed, dissociated and consume more oxygen ions (O⁻), resulting in the tendency for depletion layers to be thinner. Then slow bulk reaction process is carried out, the H atom further binds with a lattice oxygen anion in α -MoO₃ to form the adsorbed hydroxyl group.



After that, the same reactions proceed along with reactions (4) to (6).

The process leading to the response action in the bulk is represented in process (c) of Fig. 8. The overall reaction can be illustrated as:



Where O_o is the lattice oxygen, V_o²⁺ is the oxygen vacancy in the lattice. (s) and (ads) indicate surface sites and adsorbed species, respectively.

Therefore, the TEA sensing mechanism over MoO₃ is

interpreted as the transformation of triethylamine to vinylamine through catalytic oxidation, which determines the change in conductivity. As mentioned above, a large response of the sensor to TEA can be ascribed to the following four factors. Firstly, differing from a single reaction of reducing gases with the chemisorbed oxygen or the lattice oxygen, the oxidation of TEA is directed by two processes: a fast course by Eq 7 and slow course by Eq 9 since it is a bulk effect. These two processes may also proceed simultaneously, and subsequently a large number of free electrons are released by the total effect of these two reactions, leading to a huge response in conductance. Secondly, the electric conductivity of the non-stoichiometric MoO₃ is higher than stoichiometric MoO₃ because of the presence of lower valent molybdenum cation, accompanying with the formed oxygen vacancies by Eq 9. Thirdly, improvement of response of the α -MoO₃ flowers is also related to their 3D hierarchically assembled structures. The single-crystalline growth along the [001] direction of the α -MoO₃ nanobelts reveals that the building-blocks are structurally uniform and the exposed surface of (010) facets with high and special activities is advantageous for the reaction of TEA on the surface of α -MoO₃. Finally, the large specific surface area and pore volume of the α -MoO₃ flowers can supply more efficient active sites for TEA molecules to adsorb, and enhance the charge transfer from the gases to the metal oxide surface. Taking all the above factors into account, consequently a large response of the α -MoO₃ flowers sensor to TEA is observed.

Conclusions

Novel, three-dimensional, α -MoO₃ flowers with hierarchical nanostructures were prepared by a single-step, solvothermal method. Numerous high-density nanobelts with exposed (010) facets radially assembled to form the flowers. The evolution process followed a path as: 0D nanoparticles → 1D nanobelts → 3D flowers. The gas sensor based on 3D α -MoO₃ flowers showed more sensitive and selective for triethylamine (low-concentration 0.001-10 ppm) detection at the working temperature of 170°C in comparison to the sensors based on 0D α -MoO₃ nanoparticles and 1D α -MoO₃ nanobelts. The response of such sensor to 10 ppm TEA was 931.2, 8.1 and 33.7 times higher than those of α -MoO₃ nanobelts and nanoparticles, respectively. In particular, the response of the sensor to 0.001 ppm TEA attained 5.1. Moreover, we addressed the gas sensing mechanism of α -MoO₃ towards TEA, which was speculated as: the transformation of triethylamine to vinylamine through catalytic oxidation, including the TEA initial reaction with the chemisorbed oxygen and the subsequent reaction with the lattice oxygen on the surface of the α -MoO₃ flower. The sensor based on α -MoO₃ flowers is a promising candidate for instantaneous determination of ppb-ppm TEA in complex environment such as chemical industry. One important application was detection of 1 ppb TEA which is linked to the freshness of aquatic products. This work is significant for exploring α -MoO₃ nanomaterials and even other MOS with similar nanostructures for their applications in other fields.

Acknowledgments

This work was financial supported by the National Natural Science Foundation of China (61271126, 21201060 and

21305033), Program for Innovative Research Team in University (IRT-1237), Program for Science and Technology Project of Heilongjiang province (B201414, B2015008), Heilongjiang Educational Department (2013TD002, 2011CJHB006, 12531506), Youth Foundation of Harbin (2013RFQXJ142).

Notes and references

a Key Laboratory of Functional Inorganic Material Chemistry, Ministry of Education, School of Chemistry and Materials Science, Heilongjiang University, Harbin 150080, People's Republic of China. E-mail address: lhhuo68@yahoo.com; Tel.: (+86) 0451-86608426; Fax: (+86) 0451-86608040

b College of Chemistry and Chemical Engineering, Qiqihar University, Qiqihar 161006, People's Republic of China.

† Electronic Supplementary Information (ESI) available. See DOI: 10.1039/b000000x/

- X. S. Fang, L. F. Hu, C. H. Ye, and L. D. Zhang, *Pure Appl. Chem.*, 2010, **82**, 2185.
- P. Sun, W. Zhao, Y. Cao, Y. Guan, Y. F. Sun and G. Y. Lu, *CrystEngComm*, 2011, **13**, 3718.
- J. Kukkola, M. Mohl, A.-R. Leino, G. Tóth, M. C. Wu, A. Shchukarev, A. Popov, J.-P. Mikkola, J. Lauri, M. Riihimäki, J. Lappalainen, H. Jantunen and Krisztián Kordás, *J. Mater. Chem.*, 2012, **22**, 17878.
- S. C. Han, L. F. Hu, Z. Q. Liang, S. Wageh, A. A. Al-Ghamdi, Y. S. Chen and X. S. Fang, *Adv. Funct. Mater.*, 2014, **24**, 5719.
- Y. Z. Lv, C. R. Li, L. Guo, F. C. Wang, Y. Xu and X. F. Chu, *Sens. Actuators, B*, 2009, **141**, 85.
- P. Song, D. Han, H. H. Zhang, J. Li, Z. X. Yang and Q. Wang, *Sens. Actuators, B*, 2014, **196**, 434.
- A. Chithambararaj, N. S. Sanjini, A. C. Bose and S. Velmathi, *Catal. Sci. Technol.*, 2013, **3**, 1405.
- A. Chithambararaj, N. S. Sanjini, S. Velmathi and A. C. Bose, *Phys. Chem. Chem. Phys.*, 2013, **15**, 14761.
- D. L. Chen, M. N. Liu, L. Yin, T. Li, Z. Yang, X. J. Li, B. B. Fan, H. L. Wang, R. Zhang, Z. X. Li, H. L. Xu, H. X. Lu, D. Y. Yang, J. Sun and L. Gao, *J. Mater. Chem.*, 2011, **21**, 9332.
- L. Q. Wang, P. Gao, D. Bao, Y. Wang, Y. J. Chen, C. Chang, G. B. Li, and P. P. Yang, *Cryst. Growth Des.*, 2014, **14**, 569.
- D. Hanlon, C. Backes, T. M. Higgins, M. Hughes, A. O'Neill, P. King, N. McEvoy, G. S. Duesberg, B. M. Sanchez, H. Pettersson, V. Nicolosi and J. N. Coleman, *Chem. Mater.*, 2014, **26**, 1751.
- M. A. Ibrahim, F. Y. Wu, D. A. Mengistie, C. S. Chang, L. J. Li and C. W. Chu, *Nanoscale*, 2014, **6**, 5484.
- J. Zhou, N. S. Xu, S. Z. Deng, J. Chen, J. C. She and Z. L. Wang, *Adv. Mater.*, 2003, **15**, 1835.
- D. D. Yao, J. Z. Ou, K. Latham, S. Zhuyikov, A. P. O' Mullane and K. Kalantar-zadeh, *Cryst. Growth Des.*, 2012, **12**, 1865.
- A. Gavriluyuk, U. Tritthart and W. Gey, *Sol. Energ. Mat. Sol. C.*, 2011, **95**, 1846.
- E. Comini, L. Yubao, Y. Brando and G. Sberveglieri, *Chem. Phys. Lett.*, 2005, **407**, 368.
- A. K. Prasad, D. J. Kubinski and P. I. Gouma, *Sens. Actuators, B*, 2003, **93**, 25.
- M. M. Y. A. Alsaif, S. Balendhran, M. R. Field, K. Latham, W. Wlodarski, J. Z. Ou and K. Kalantar-zadeh, *Sens. Actuators, B*, 2014, **192**, 196.
- Y. H. Cho, Y. N. Ko, Y. C. Kang, Il-D. Kim and J-H. Lee, *Sens. Actuators, B*, 2014, **195**, 189.
- S. Barazzouk, R. P. Tandon and S. Hotchandani, *Sens. Actuators, B*, 2006, **119**, 691.
- N. Illyaskutty, H. Kohler, T. Trautmann, M. Schwotzer and V. P. M. Pillai, *Sens. Actuators, B*, 2013, **187**, 611.
- S. L. Yang, Z. Wang, Y. M. Hu, X. T. Luo, J. M. Lei, D. Zhou, L. F. Fei, Y. Wang and H. S. Gu, *ACS Appl. Mater. Interfaces*, 2015, **7**, 9247.
- L. Xu, H. J. Song, J. Hu, Y. Lv and K. L. Xu, *Sens. Actuators, B*, 2012, **169**, 261.
- W. H. Zhang and W. D. Zhang, *Sens. Actuators, B*, 2008, **134**, 403.

- 25 M. Z. Wu, X. F. Zhang, S. Gao, X. L. Cheng, Z. M. Rong, Y. M. Xu, H. Zhao and L. H. Huo, *CrystEngComm*, 2013, **15**, 10123.
- 26 Y. J. Xie, J. P. Du, R. H. Zhao, H. Y. Wang and H. L. Yao, *J. Environ. Chem. Eng.*, 2013, **1**, 1380.
- 5 27 H. K. Wang, F. Fu, F. H. Zhang, H. E. Wang, S. V. Kershaw, J. Q. Xu, S. G. Sun and A. L. Rogach, *J. Mater. Chem.*, 2012, **22**, 2140.
- 28 F. Song, H. L. Su, J. J. Chen, W.-J. Moon, W. M. Lau and D. Zhang, *J. Mater. Chem.*, 2012, **22**, 1121.
- 29 M. R. Alenezi, S. J. Henley, N. G. Emerson and S. R. P. Silva, *Nanoscale*, 2014, **6**, 235.
- 10 30 H. J. Zhang, R. F. Wu, Z. W. Chen, G. Liu, Z. N. Zhang and Z. Jiao, *CrystEngComm*, 2012, **14**, 1775.
- 31 S. L. Bai, K. W. Zhang, L. S. Wang, J. H. Sun, R. X. Luo, D. Q. Li and A. F. Chen, *J. Mater. Chem. A*, 2014, **2**, 7927.
- 15 32 H. J. Song, X. H. Jia, H. Qi, X. F. Yang, H. Tang and C. Y. Min, *J. Mater. Chem.*, 2012, **22**, 3508.
- 33 S. M. Wang, B. X. Xiao, T. Y. Yang, P. Wang, C. H. Xiao, Z. F. Li, R. Zhao and M. Z. Zhang, *J. Mater. Chem. A*, 2014, **2**, 6598.
- 34 Y. L. Ge, K. Kan, Y. Yang, L. Zhou, L. Q. Jing, P. K. Shen, L. Li and K. Y. Shi, *J. Mater. Chem. A*, 2014, **2**, 4961.
- 20 35 J. N. Deng, L. L. Wang, Z. Lou and T. Zhang, *RSC Adv.*, 2014, **4**, 21115.
- 36 X. Y. Yu, G. X. Zhang, Z. Y. Lu, J. F. Liu, X. D. Lei and X. M. Sun, *CrystEngComm*, 2014, **16**, 3935.
- 25 37 G. C. Li, L. Jiang, S. P. Pang, H. G. Peng and Z. K. Zhang, *J. Phys. Chem. B*, 2006, **110**, 24472.
- 38 S. T. Wang, Y. G. Zhang, X. C. Ma, W. Z. Wang, X. B. Li, Z. D. Zhang and Y. T. Qian, *Solid State Commun.*, 2005, **136**, 283.
- 39 G. D. Wei, W. P. Qin, D. S. Zhang, G. F. Wang, R. Kim, K. Z. Zheng and L. L. Wang, *J. Alloy. Compd.*, 2009, **481**, 417.
- 30 40 L. L. Cai, P. M. Rao and X. L. Zheng, *Nano Lett.*, 2011, **11**, 872.
- 41 L. Fang, Y. Y. Shu, A. Q. Wang and T. Zhang, *J. Cryst. Growth*, 2008, **310**, 4593.
- 42 L. L. Sui, Y. M. Xu, X. F. Zhang, X. L. Cheng, S. Gao, H. Zhao, Z. Cai and L. H. Huo, *Sens. Actuators, B*, 2015, **208**, 406.
- 35 43 J. Li and X. H. Liu, *CrystEngComm*, 2014, **16**, 184.
- 44 J. S. Chen, Y. L. Tan, C. M. Li, Y. L. Cheah, D. Y. Luan, S. Madhavi, F. Y. C. Boey, L. A. Archer and X. W. Lou, *J. Am. Chem. Soc.*, 2010, **132**, 6124.
- 40 45 X. G. Han, Q. Kuang, M. S. Jin, Z. X. Xie and L. S. Zheng, *J. Am. Chem. Soc.*, 2009, **131**, 3152.
- 46 X. L. Li, W. J. Wei, S. Z. Wang, L. Kuai and B. Y. Geng, *Nanoscale*, 2011, **3**, 718.
- 47 X. H. Liu, J. Zhang, S. H. Wu, D. J. Yang, P. R. Liu, H. M. Zhang, S. R. Wang, X. D. Yao, G. S. Zhu and H. J. Zhao, *RSC Adv.*, 2012, **2**, 6178.
- 45 48 S. Pokhrel, L. H. Huo, H. Zhao and S. Gao, *Sens. Actuators, B*, 2007, **120**, 560.
- 49 H. Ma, Y. M. Xu, Z. M. Rong, X. L. Cheng, S. Gao, X. F. Zhang, H. Zhao and L. H. Huo, *Sens. Actuators, B*, 2012, **174**, 325.
- 50 50 R. L. Liang, H. Q. Cao and D. Qian, *Chem. Commun.*, 2011, **47**, 10305.
- 51 X. F. Chu, D. L. Jiang, Y. Guo and C. M. Zheng, *Sens. Actuators, B*, 2006, **120**, 177.
- 55 52 D. Wang, X. F. Chu and M. L. Gong, *Sens. Actuators, B*, 2006, **117**, 183.
- 53 X. F. Chu, D. L. Jiang and C. M. Zheng, *Sens. Actuators, B*, 2007, **123**, 793.
- 54 F. H. Zhang, H. Q. Yang, X. L. Xie, L. Li, L. H. Zhang, J. Yu, H. Zhao and B. Liu, *Sens. Actuators, B*, 2009, **141**, 381.
- 60 55 H. Y. Yang, X. L. Cheng, X. F. Zhang, Z. K. Zheng, X. F. Tang, Y. M. Xu, S. Gao, H. Zhao and L. H. Huo, *Sens. Actuators, B*, 2014, **205**, 322.
- 56 S. S. Sunu, E. Prabhu, V. Jayaraman, K. I. Gnanasekar, T. K. Seshagiri and T. Gnanasekaran, *Sens. Actuators, B*, 2004, **101**, 161.
- 65 57 X. L. Cheng, Z. M. Rong, X. F. Zhang, Y. M. Xu, S. Gao, H. Zhao and L. H. Huo, *Sens. Actuators, B*, 2013, **188**, 425.
- 58 N. Illyaskutty, H. Kohler, T. Trautmann, M. Schwotzerc and V. P. M. Pillai, *J. Mater. Chem. C*, 2013, **1**, 3976.
- 70 59 J. R. D. L. Fuente, C. Jullian, C. Saitz and V. Neira, *J. Org. Chem.*, 2005, **70**, 8712.
- 60 X. F. Chu, T. Y. Chen, W. B. Zhang, B. Q. Zheng and H. F. Shui, *Sens. Actuators, B*, 2009, **142**, 49.

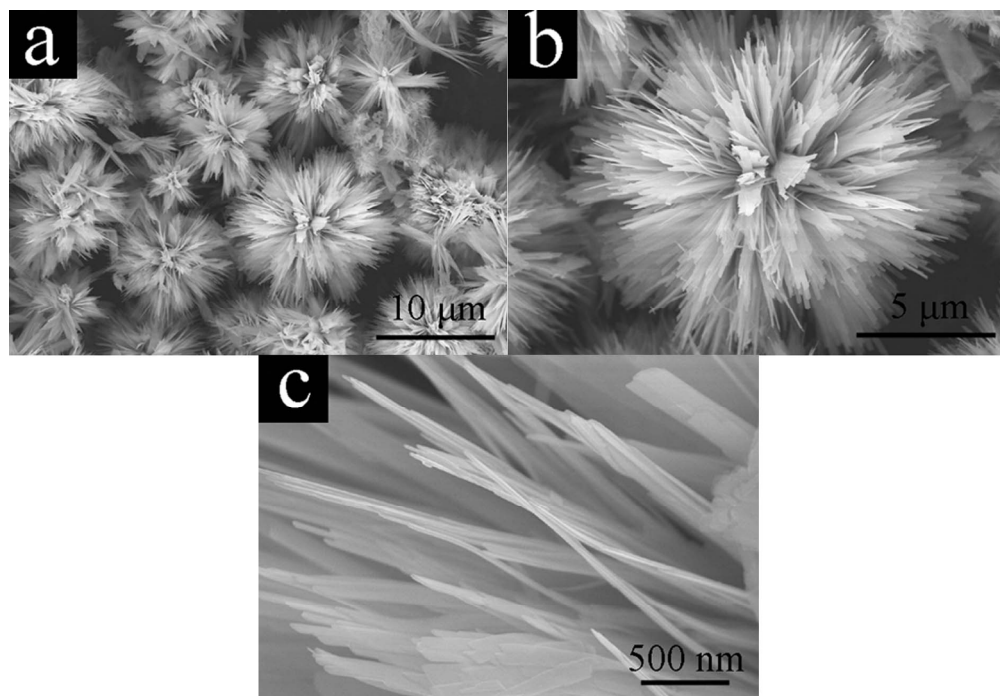


Figure 1. Typical SEM images of α -MoO₃ product prepared for 8 h.
160x110mm (300 x 300 DPI)

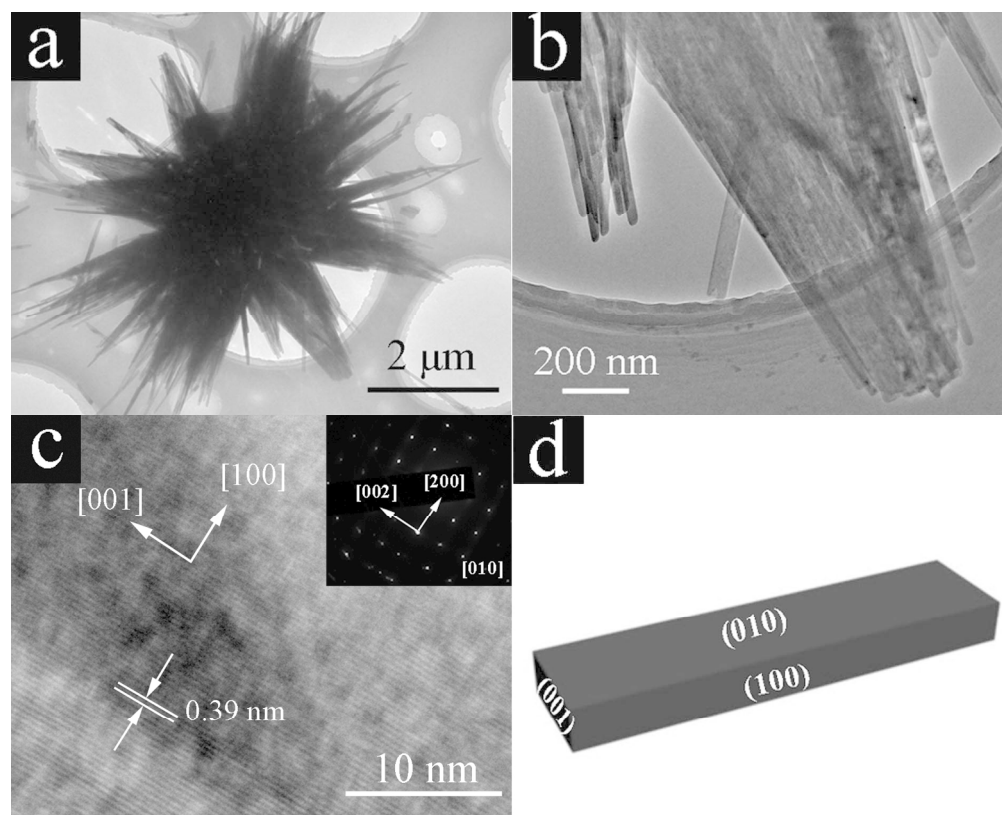


Figure 2. Typical TEM (a and b), HRTEM (c) images, SAED pattern (inset of c) of α - MoO_3 flower-like hierarchical nanostructure and α - MoO_3 nanobelt with different growth directions (d).
160x129mm (300 x 300 DPI)

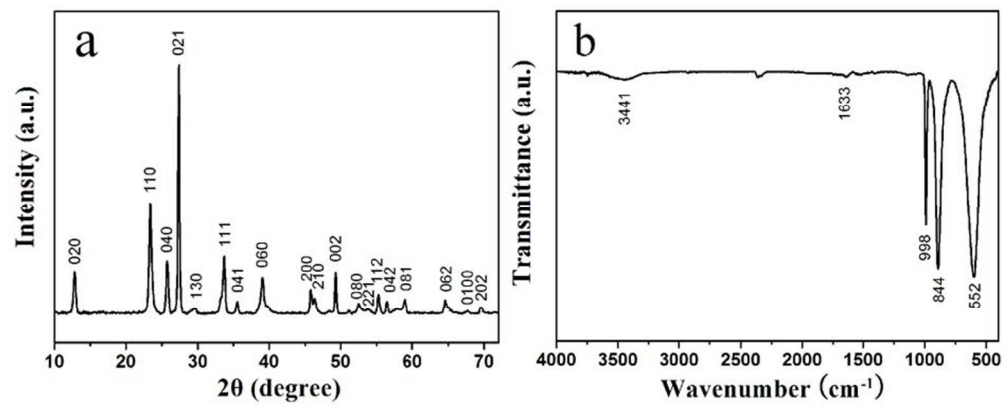


Figure 3. XRD pattern (a) and FT-IR spectrum (b) of the product prepared for 8 h.
80x32mm (300 x 300 DPI)

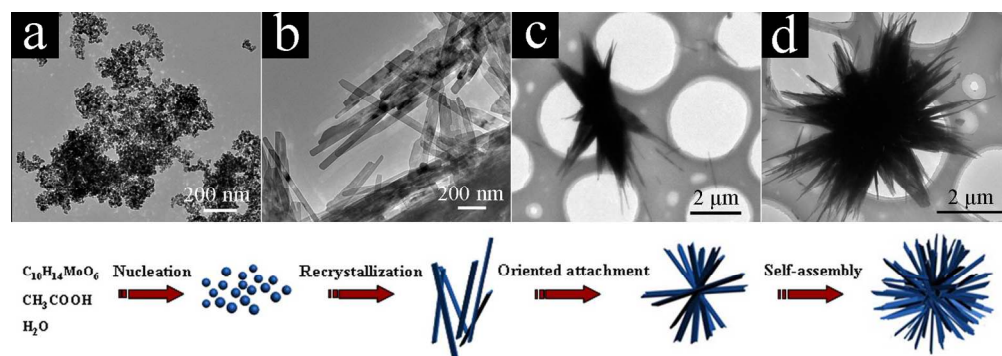


Figure 4. TEM micrographs of the intermediate products collected at different reaction stages: 5 min (a), 30 min (b), 2 h (c), 8 h (d) and the corresponding schematic formation process of the α -MoO₃ flower.
160x56mm (300 x 300 DPI)

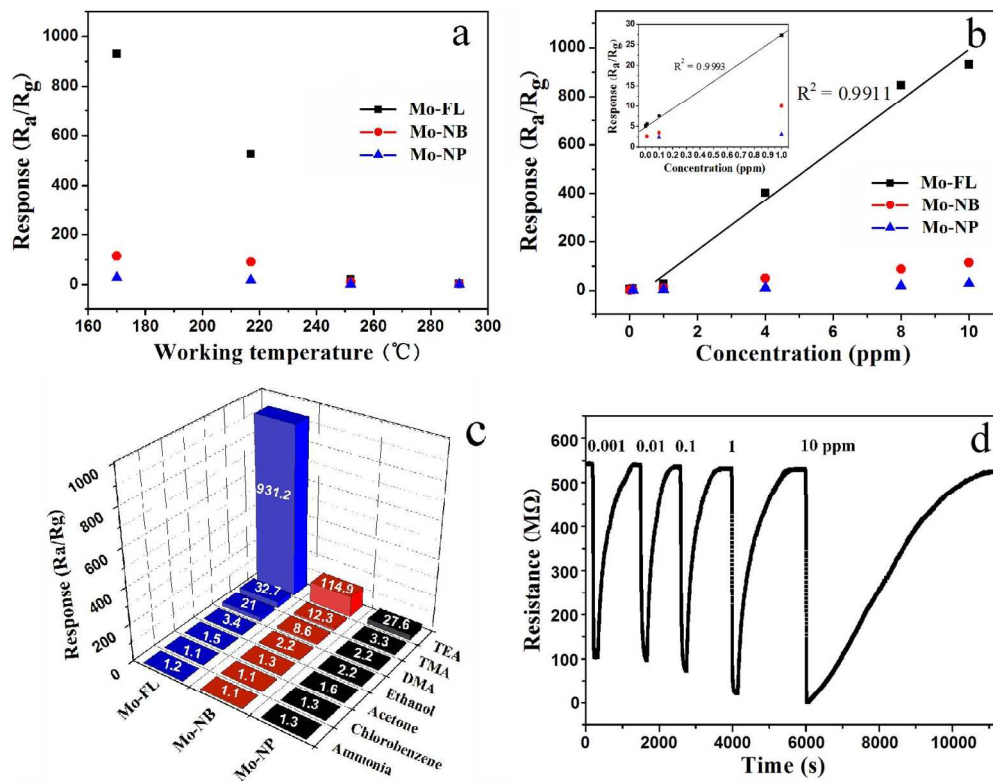


Figure 5. The responses of Mo-NP, Mo-NB and Mo-FL sensors versus the working temperatures to 10 ppm TEA gas (a), versus the concentration of TEA gas (b), versus 10 ppm various gases (c); sensing transients of Mo-FL sensor to 0.001-10 ppm TEA (d) at 170 °C.
160x125mm (300 x 300 DPI)

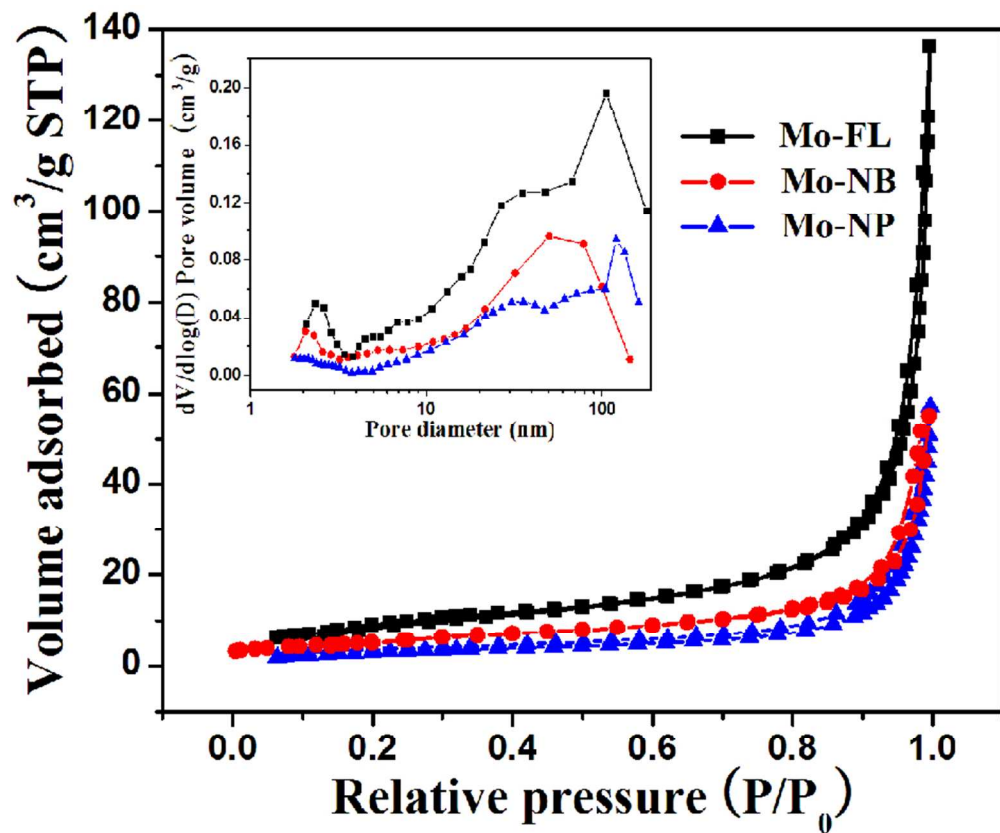


Figure 6. Typical nitrogen adsorption-desorption isotherms and BJH pore size distribution plots (inset) of Mo-NP, Mo-NB and Mo-FL materials.
80x66mm (300 x 300 DPI)

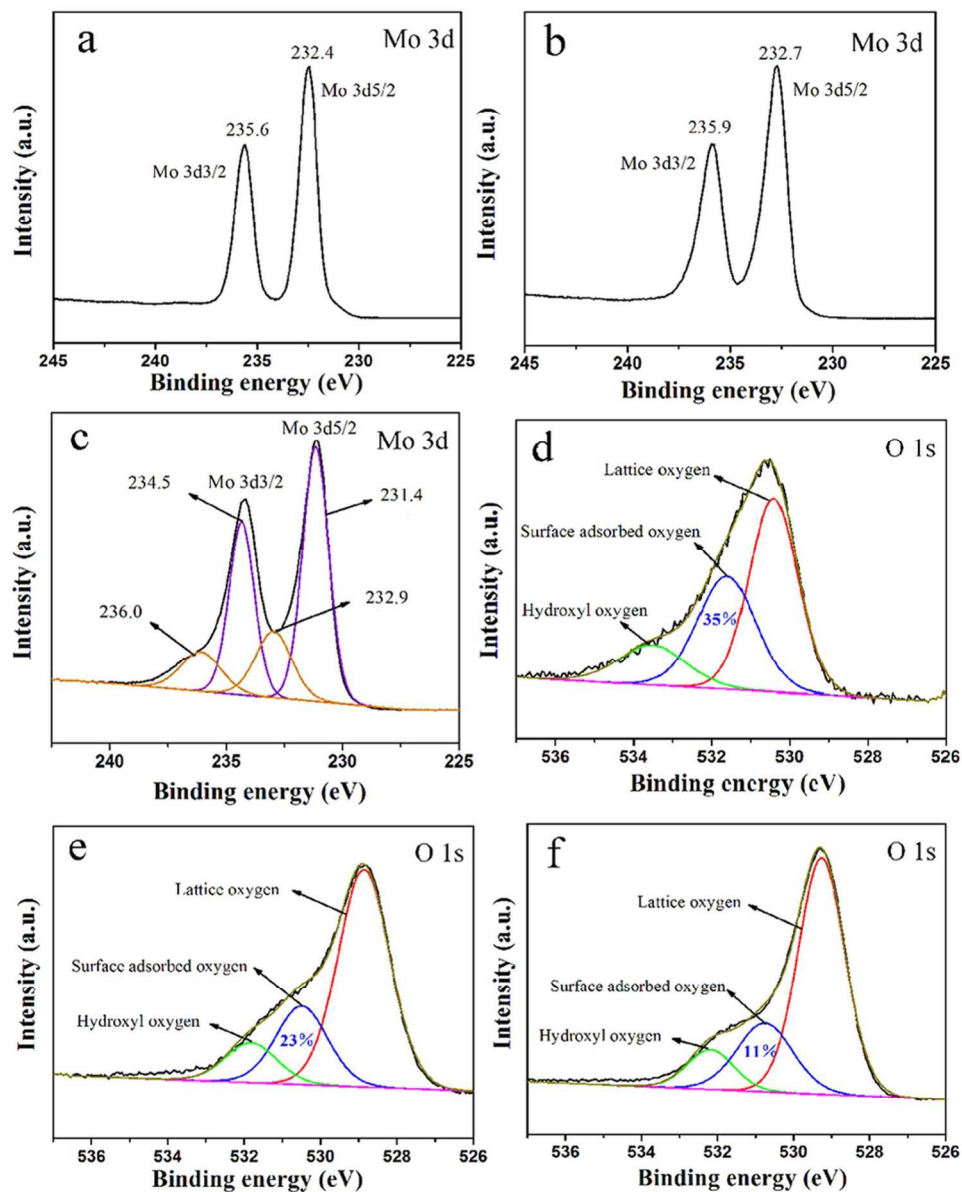


Figure 7. Mo 3d/O 1s XPS spectra of α -MoO₃ flowers before (a)/(d) and after the sensor exposure to 0.01 ppm (b)/(e) and 10 ppm (c)/(f) TEA at 170 °C.
160x200mm (300 x 300 DPI)

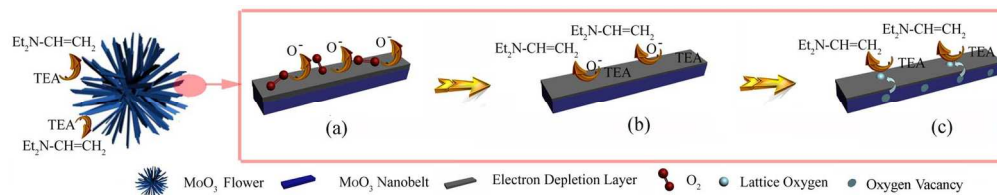


Figure 8. Schematic diagrams on the gas sensing mechanism of flower-like α - MoO_3 hierarchical nanostructures: the formation process of chemisorbed oxygen (a), the subsequent surface reaction process (b) and bulk reaction process (c).
160x30mm (300 x 300 DPI)

Table 1 Sensing responses of α -MoO₃ to 10 ppm TEA in this work and other reported sensing materials.

Sensing material	Working temperature (°C)	Response (<i>Ra/Rg</i>)	Detection limit (ppm)	Year and reference
Flower-like α -MoO ₃	170	931.2	0.001	In this work
α -MoO ₃ nanobelts	170	114.9	0.01	In this work
α -MoO ₃ nanoparticles	170	27.6	0.1	In this work
α -MoO ₃ flowers	250	9.7	0.5	2015 [42]
CoFe ₂ O ₄ nano-crystallines	190	2	—	2006 [51]
SnO ₂ nanorods	350	65	—	2006 [52]
NiFe ₂ O ₄ nanorods	175	30	—	2007 [53]
Sea urchin-like α -Fe ₂ O ₃	350	6	—	2009 [54]
TiO ₂ nanorod arrays	290	2.7	0.1	2014 [55]
ZnO nanorods	150	70	0.001	2009 [5]
V ₂ O ₅ hollow spheres	370	2.9	0.01	2013 [25]
Hexagonal brick-shaped SnO ₂	160	14	—	2013 [26]